Modeling two loops RLC circuit AC power source using symbolic arithmetic differential equations

Inaam Rikan Hassan[1], Ghuson S. Abed[2], Ahmad H. Sabry[3]
[1]Department of Scholarships and Cultural Relations, University of Information Technology and Communications (UOITC), Baghdad, Iraq
[2]Department of Media Technology and Communications Engineering, University of Information Technology and Communications (UOITC), Baghdad, Iraq
[3]Department of Computer Engineering, Engineering Collage, Al-Nahrain University, Baghdad, Iraq

Article Info

Article history:

Received Nov 23, 2022
Revised Apr 17, 2023
Accepted May 3, 2023

Keywords:

Convolutional neural network
Deep learning
Electrical circuits
Linear differential equations
Laplace transform
Second order

ABSTRACT

As oscillator applications, resistance-inductor-capacitor (RLC) circuits are employed in a diversity of settings. A low-pass, band-stop, band-pass, or high-pass filters can all be designed using an RLC circuit. A two-loop RLC circuit could not be represented mathematically in prior studies. Laplace transform is one type of integral transformation, which is able to resolve both second order non-uniform and uniform linear differential equations. This work solves the differential equations (DEs) of a two loops RLC circuit of an alternating voltage source by using two alternative approaches, Laplace transform (LT) and deep learning convolutional neural network (DLCNN). Initially, two DE have been declared. Next, Laplace transform is computed to solve these equations with symbolic variables for the first loop current and capacitor charge. Finally, we substitute the numerical values of the circuit elements for the symbolic variables. The charge and current initially decline exponentially. On the other hand, they oscillate over a long period of time. The capacitor charge and current initially decline exponentially and oscillate over a long period of time. The qualities of the result can be examined with a symbolic result, which is not possible with a numeric result.

Corresponding Author:

Ahmad H. Sabry
Department of Computer Engineering, Engineering Collage, Al-Nahrain University
Baghdad, Iraq
Email: ahs4771384@gmail.com

1. INTRODUCTION

Due to experimental or numerical analyses on the behavior between a dissipative and conservative system and the absence of fractionalized systematic techniques, recent research has been diverted from the importance of the recent fractional derivatives including the non-singular kernel with non-locality and the singular kernel with the locality. The mathematical representation of an ordinary differential equation (DE) with second-order cubic nonlinearity is the Van-der-Pol equation. The Van-der-Pol equation has been given a time delay in several investigations. Theresistor-inductor-capacitor (RLC) circuit differential equation is derived as a delay differential equation in this study together with the Van der Pol model differential equation [1]. Analytical solutions for the Caputo-Fabrizio, Liouville-Caputo, and new Mittag-Leffler function-based fractional derivative to describe the electrical RLC circuit model were previously discussed. The fractional differential equations take different sources into account. When the fractional order equals 1, the conventional behaviors are restored [2]. Dynamical system approaches and Melnikov theory can be used to examine tiny amplitude perturbations of some implicit differential equations appearing in RLC circuits [3]. A steady-state process in an RLC circuit with power sources operating at unrelated frequencies is also considered [4]. An expansion of an ordinary differential equation is taken into consideration in order to achieve the periodic steady-state behavior. This expansion is based on changing from ordinary differential equations to partial differential equations with two-time variables by adding an additional time variable. The two-dimensional Laplace transform is used to solve the obtained differential equations. Active power and frequency responses for the domain of two time variables are specified by the use of double integral formulas for a transfer function. The voltage and current amplitude-frequency properties of the RLC circuit can be given in the domain of two variables. A nonlinear fractional derivative based Volterra integral-differential equation with Caputo, several kernels, and numerous constant delays is also considered to look into the qualitative properties of solutions to this equation, including the boundedness of nonzero solutions and the Mittag-Leffler stability, uniform stability, and asymptotic stability of the zero solution [5]. The Lyapunov-Razumikhin approach and selecting an acceptable Lyapunov function are the methods employed in the proofs of these theorems related to an RLC circuit.

A modified Laplace transform approach to find solutions to a series-connected simple electric circuits (RLC) model of linear differential equations (DEs) was presented in [6]. Although the study suggested that non-homogenous second order linear differential equations in the form of electric charge equations can be solved over time using a modified Laplace transform method, only homogeneous second order linear DEs was considered. Certain approximation techniques for generated nonlinear terms of characteristic exponents to offer the stability analysis of delay integral-differential equations with fractional order derivatives were discussed in [7]. Such methods allow for the proof of the presence of some analytical solutions close to their equilibrium points. The formulas for the critical time delay and critical frequency are determined through the construction of stability charts to describe general RLC circuits that expose the delay and fractional order derivatives. A straightforward method was used to determine the electromagnetic energy density distribution in a dispersive and dissipative met material made up of wire arrays and split-ring resonators [8]. The paper demonstrated that the system's energy may be thought of as being made up of the energy densities of the electric and magnetic fields as well as energy densities associated with the medium's reaction. Therefore, the system's equations of motion for polarization have been compared with the corresponding differential equations of suitable RLC circuits to develop formulas for the energy density of the medium. The electrical RLC circuit with a fractional DE is investigated in [9], where a new auxiliary parameter was added to maintain the three physical measures C, L, and R's three dimensions. Through the circuit's physical properties of RLC, the analytical solution was specified in terms of Mittag-Leffler's formula. An analytical approach to examine the impacts of contemporary fractional differentiation on the RLC electrical circuit was discussed in [10]. The leading RLC electrical circuit DE has been fractionalized with three kinds of partial derivatives, where the RLC electrical circuit was seen for unit step sources, periodic, and exponential.

Melnikov's theory for implied ordinary DEs of little amplitude perturbations was presented in [11]. If certain Melnikov-like criteria are met, it is specifically explored how long orbits linking singularities can endure in finite time for nonlinear RLC circuit systems. The two delays in the Van der Pol delay model and delay differential equations were produced from ordinary differential equations using the Taylor series to define the model for treating Parkinson's disease [1]. Floquet's theory to examine the linear dynamic analysis of RLC circuits representing AC generators with periodically time-varying inductances was presented in [12]. The dynamic stability's prerequisites are derived. The stability domains and transition curves were predicted using the harmonic balancing approach. A fractional order differential equation can be used to describe the dynamics of noninteger order RLC electrical circuits by adding an auxiliary parameter [13], where an analytical determination of the filter parameters and numerical validation of the outcomes were used. Despite the fact that differential equations are marketed as applied mathematics, the course rarely includes any practical applications [14]. Deep learning convolutional neural networks (DLCNN) [15]–[18] and reinforcement learning [19], [20] that were undergone fast growth in modern decades, were employed to solve the nonlinear DEs in general. Deep learning-based data assimilation algorithms [21], [22] were lately presented to train Navier–Stokes network formulas to estimate different quantities of interesting. DLCNN-based methods can be classified into three kinds: i) DLCNN that maps indirectly to the parameters or inner results of an algebraic explanation to use them for deriving numerical solutions [23], [24]; ii) DLCNN that maps directly toward the solutions with a discrete method, which is same as numerical solutions [25], [26]; and iii) DLCNN that maps straight to the solution characterized by a DLCNN with a continuous way and it is similar to that in analytical solutions [27]–[29]. In this type, the data applied for training the network are arbitrarily modeled inside the whole solution range in every training batch, including boundary and initial circumstances. The necessary characteristic of all of these techniques is the adopting the benefit of the nonlinearity depiction capability of DLCNNs. New development [30] in mechanics with this capability has been stated such as, Li *et al*. [31] presented a generative adversarial model network for mapping hidden variables for a microstructure to use in fabrication. The major contribution of this work is to model the DEs of a two loops RLC circuit of an alternating voltage AC-source by using two alternative approaches; Laplace transform and DLCNN in MATLAB environment. To obtain this aim, several objectives are accomplished such as: i) to model and solve the DEs of a 2-loop RLC AC circuit; ii) to plot and analyze the obtained results of the capacitor charging and inductor current; and iii) to solve and compare the results with the DLCNN-based solution.

2. METHOD

2.1. Object and research hypothesis

This work solves the RLC circuit differential equations by using Laplace transform. It is possible to define the Laplace transform by a function $f(t)$, which is given by:

$$\int_0^\infty f(t)\, e^{-ts} dt$$

Calculations are kept in their native symbolic form rather than in numerical form using symbolic workflows. This method enables using precise symbolic values and comprehends the properties of the obtained answer. When a quantitative result is required or symbolically continuing is impossible, numbers are substituted for symbolic variables. In general, the symbolic workflows of solving equations include; equations definition, equations solving, values substitution, plotting results, and analyzing results.

2.2. Equations definition

To solve differential equations using beginning conditions, utilize the Laplace transform. We will consider solving the RLC circuit shown in Figure 1. Capacitor charge is referred to as $Q(t)$ in coulomb, AC voltage source in volts is referred to as $E(t)$, capacitance in farad is referred to as C, inductance in henry is referred to as L, currents in ampere are referred as I1, I2, I3, resistances in ohm are referred as R1, R2, R3. Apply Kirchhoff's current and voltage laws, following equations, are obtained:

$$\begin{aligned} &I_1 = I_2 + I_3 \\ &L\frac{dI_1}{dt} + I_1R_2 + I_2R_2 = 0 \\ &E(t) + I_2R_2 - \frac{Q}{C} - I_3R_3 = 0 \end{aligned} \tag{1}$$

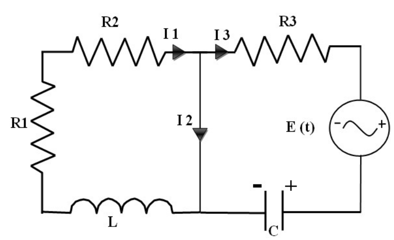

Figure 1. RLC circuit analysis

By substituting the term $I3 = dQ/dt$ (which represents the rate of charge of the capacitor) into $eqn(1)$, the following differential equations are obtained for the RLC circuit:

$$\begin{aligned} &\frac{dI_1}{dt} - \frac{R_2dQ}{Ldt} = -\frac{R_1+R_2}{L}I_1 \\ &\frac{dQ}{dt} = \frac{1}{R_2+R_3}\left(E(t) - \frac{Q}{C}\right) + \frac{R_2}{R_2+R_3}I_1 \end{aligned} \tag{2}$$

Since the magnitude of the practical components are with positive quantities, we stat the variables of equations. Then, we set the equivalent statements for the variables. Suppose that $E(t)$is a 1 V AC source voltage ($1.sin(t)$), and assuming t, L, C, and R are greater than 0. Therefore, the differential equations are:

$$eqn1(t) = \frac{\partial}{\partial t} I_1(t) - \frac{R_2 \frac{\partial}{\partial t} Q(t)}{L} = -\frac{I_1(t)(R_1+R_2)}{L} \tag{3}$$

$$eqn2(t) = \frac{\partial}{\partial t}\, Q(t) = \frac{sin(t) - \frac{Q(t)}{c}}{R_2+R_3} + \frac{R_2 I_1(t)}{R_2+R_3} \tag{4}$$

2.3. Deep learning convolutional neural network framework

From a physical perspective, the initial and boundary circumstances are continued with time, and as a result, the parameters of the approach circuit are also continuous in time: the parameters at the current step are used as an ideal initialization for the next step, allowing the parameters of the DLCNN to transmit with the time phase in the solution procedure, which makes the process rapid for the remaining time stages. The derivatives of the current and capacitor charge equations are computed according to the gradient of the network output according to the input. The hidden layers activation functions are selected as rectified linear unit (ReLU) functions to conserve the stability of those derivatives. The network architecture is trained according to the computed loss based on the gradient descent process. A common nonlinear differential equation has the following format:

$$u_t + N(u, \vartheta) = 0 \tag{5}$$

The term $u(x,t)$ represents the underlying equation solution, u_t represents the time derivative, while $N(u, \vartheta)$ denotes the nonlinear function with parameter ϑ. Specifying the required condition, represented by the initial and boundary parameters, the equation solution is a nonlinear map within the solution range (x, t). DLCNNs have revealed noteworthy achievements in the learning of nonlinear high-dimensional functions [32]. The proposed DLCNN technique approximates the nonlinearity mapping that has a probabilistic network $\pi_\theta(a|s)$ employed through a DLCNN with the parameter θ. The contender solution is sampled from the network probability, which means $\hat{u} \sim \pi_\theta(a|s)$. The network's loss function for continuous solution action domain. The symbols employed here are recognizable from traditional DLCNN learning for simplicity, and Figure 2 shows how they apply to a particular solution problem.

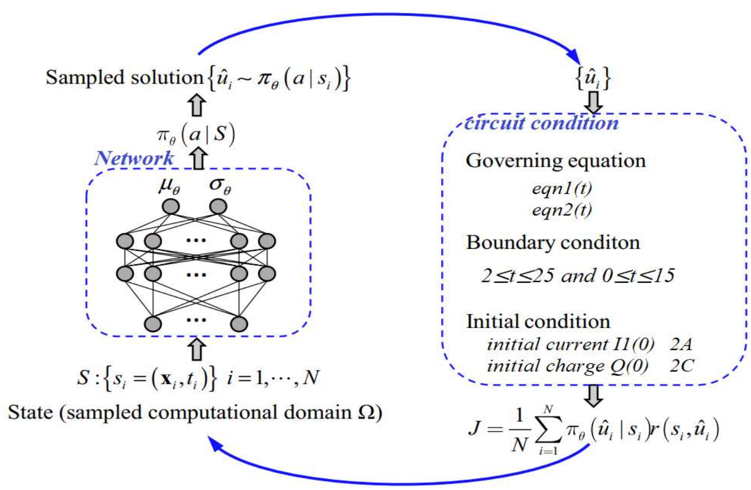

Figure 2. DLCNN framework for the DEs of the adopted two-loop RLC circuit

This research uses a DLCNN with six convolution layers and one fully linked layer. A max pooling layer, activation layer (linear rectified unit, or ReLU), and normalization batch layer are present in every convolution layer, with the exception of the final convolution level, when an average pooling level is utilized in place of the maximum layer. In the output layer, softmax activation is present. Figure 3 displays the screenshot for the specifics of the created network layers. The training configuration are: i) every nine epochs, the learning rate is decreased by a factor of 10; ii) setting the initial learning rate to 2e-2; iii) setting the maximum number of epochs to 12; iv) using a stochastic gradient descent with momentum (SGDM) solver with a mini-batch size of 256; and v) plotting the training progress.

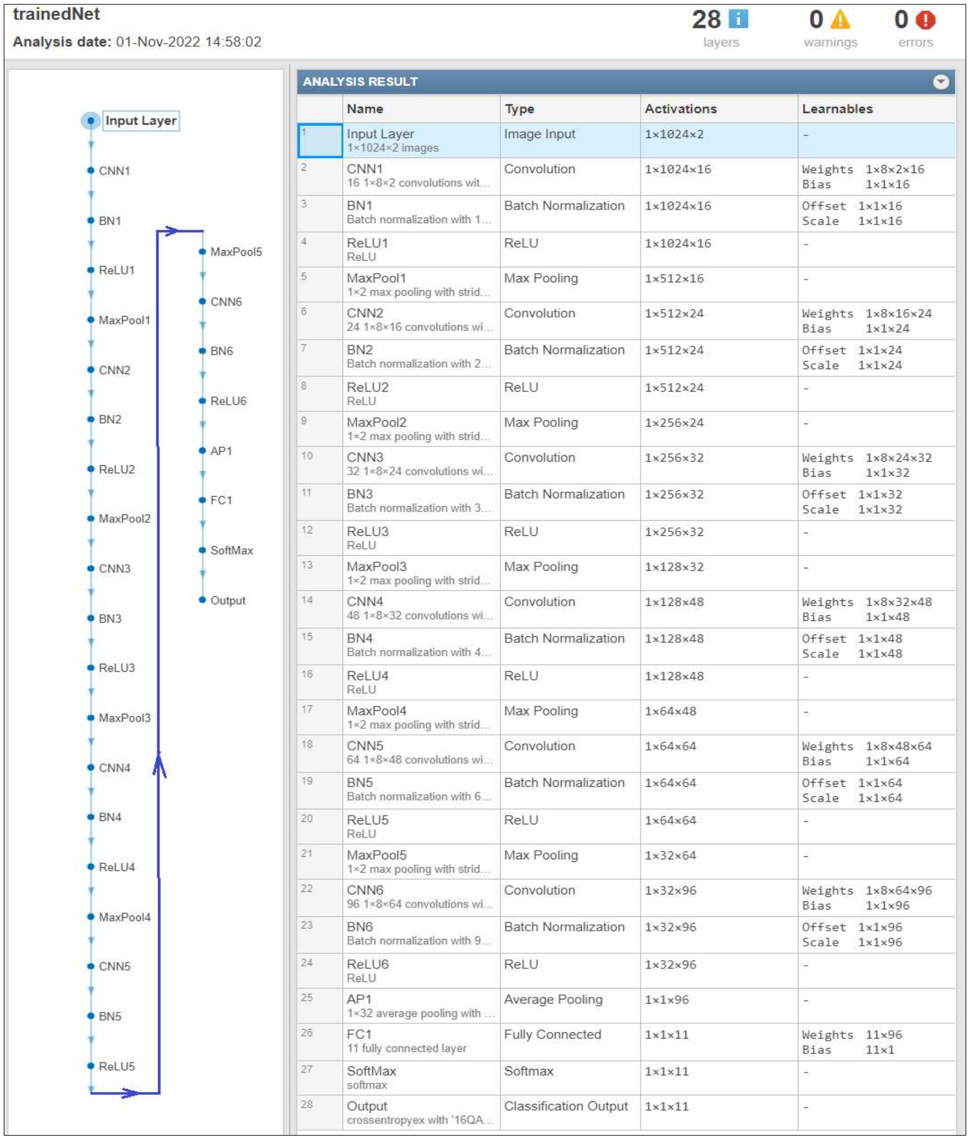

	Name	Type	Activations	Learnables
1	Input Layer 1×1024×2 images	Image Input	1×1024×2	-
2	CNN1 16 1×8×2 convolutions wit...	Convolution	1×1024×16	Weights 1×8×2×16 Bias 1×1×16
3	BN1 Batch normalization with 1...	Batch Normalization	1×1024×16	Offset 1×1×16 Scale 1×1×16
4	ReLU1 ReLU	ReLU	1×1024×16	-
5	MaxPool1 1×2 max pooling with strid...	Max Pooling	1×512×16	-
6	CNN2 24 1×8×16 convolutions wi...	Convolution	1×512×24	Weights 1×8×16×24 Bias 1×1×24
7	BN2 Batch normalization with 2...	Batch Normalization	1×512×24	Offset 1×1×24 Scale 1×1×24
8	ReLU2 ReLU	ReLU	1×512×24	-
9	MaxPool2 1×2 max pooling with strid...	Max Pooling	1×256×24	-
10	CNN3 32 1×8×24 convolutions wi...	Convolution	1×256×32	Weights 1×8×24×32 Bias 1×1×32
11	BN3 Batch normalization with 3...	Batch Normalization	1×256×32	Offset 1×1×32 Scale 1×1×32
12	ReLU3 ReLU	ReLU	1×256×32	-
13	MaxPool3 1×2 max pooling with strid...	Max Pooling	1×128×32	-
14	CNN4 48 1×8×32 convolutions wi...	Convolution	1×128×48	Weights 1×8×32×48 Bias 1×1×48
15	BN4 Batch normalization with 4...	Batch Normalization	1×128×48	Offset 1×1×48 Scale 1×1×48
16	ReLU4 ReLU	ReLU	1×128×48	-
17	MaxPool4 1×2 max pooling with strid...	Max Pooling	1×64×48	-
18	CNN5 64 1×8×48 convolutions wi...	Convolution	1×64×64	Weights 1×8×48×64 Bias 1×1×64
19	BN5 Batch normalization with 6...	Batch Normalization	1×64×64	Offset 1×1×64 Scale 1×1×64
20	ReLU5 ReLU	ReLU	1×64×64	-
21	MaxPool5 1×2 max pooling with strid...	Max Pooling	1×32×64	-
22	CNN6 96 1×8×64 convolutions wi...	Convolution	1×32×96	Weights 1×8×64×96 Bias 1×1×96
23	BN6 Batch normalization with 9...	Batch Normalization	1×32×96	Offset 1×1×96 Scale 1×1×96
24	ReLU6 ReLU	ReLU	1×32×96	-
25	AP1 1×32 average pooling with ...	Average Pooling	1×1×96	-
26	FC1 11 fully connected layer	Fully Connected	1×1×11	Weights 11×96 Bias 11×1
27	SoftMax softmax	Softmax	1×1×11	-
28	Output crossentropyex with '16QA...	Classification Output	1×1×11	-

Figure 3. Screenshot for the details of the developed network layers

3. RESULTS AND DISCUSSION

3.1. Equations'solving

The Laplace transform is calculate for $eqn1$ and $eqn2$ as:

$$eqn1LT \; = laplace(eqn1, t, s) =$$
$$Iaplace(I_1(t), t, s) - I_1(0) + \frac{R_2(Q(0) - s\, laplace(Q(t), t, s))}{L} = -\frac{(R_1 + R_2) laplace(I_1(t), t, s)}{L} \tag{6}$$

$$eqn2LT \; = laplace(eqn2, t, s) =$$
$$s\, laplace(Q(t), t, s) - Q(0) = \frac{R_2 laplace(I_1(t), t, s)}{(R_2 + R_3)} + \frac{\frac{C}{s^2+1} - laplace(Q(t), t, s)}{c\,(R_2 + R_3)} \tag{7}$$

By substituting Laplace $laplace(Q(t), t, s)$ and $(I1(t), t, s)$ by the variables Q_LT and $I1\_LT$ we get:

$$eqn1LT \; = \; I_{1,LT}s - I_1(0) + \frac{R_2(Q(0) - Q_{LT}s)}{L} = -\frac{I_{1,LT}(R_1 + R_2)}{L} \tag{8}$$

$$eqn2LT = Q_{1,LT}s - Q(0) = \frac{I_{1,LT}R_2}{R_2+R_3} - \frac{Q_{LT}-\frac{C}{s^2+1}}{c\,(R_2+R_3)} \tag{9}$$

Solving the equations for Q_LT and $I1\_LT$ we get:

$$I1-LT = \frac{\begin{array}{c}LI_1(0)-R_2Q(0)+CR_2s+Ls^2\,I_1(0)-R_2s^2\,Q(0)+C\,L\,R_2s^3\,I_1(0)+\\ C\,L\,R_3s^3\,I_1(0)+C\,L\,R_3sI_1(0)+C\,(R_1+R_2+Ls+L\,R_2I_1(0)+R_1R_2Q(0)\end{array}}{(s^2+1)(R_1+R_2+Ls+C\,L\,R_2s^2+C\,L\,R_3s^2+C\,R_1\,R_2s+C\,R_1\,R_3s+C\,R_2\,R_3s\;\;)}$$

$$\frac{\begin{array}{c}+R_1R_3Q(0)+R_2R_3Q(0)+L\,R_2s^2\,I_1(0)+L\,R_2s^3\,Q(0)+L\,R_3s^3\,Q(0)+R_1R_2s^2\,Q(0)+\\ R_1R_3s^2\,Q(0)+R_1R_3s^2\,Q(0)+L\,R_2s\,Q(0)+L\,R_3s\,Q(0)\end{array}}{(s^2+1)(R_1+R_2+Ls+C\,L\,R_2s^2+C\,L\,R_3s^2+C\,R_1\,R_2s+C\,R_1\,R_3s+C\,R_2\,R_3s\;\;)} \tag{10}$$

Calculate Q and $I1$ by calculating the inverse Laplace transform of Q_LT and $I1\_LT$. Then simplifying the answer and substituting the symbolic variables with the circuit element values as listed in Table 1 to get I_{1sol} and Q_{sol}.

Table 1. The symbolic variables with the circuit element values

Description	Value
R1	4 Ω
R2	2 Ω
R3	3 Ω
L	1.6 H
C	¼ F
Initial current $I1(0)$	2 A
Initial charge $Q(0)$	2 C

$$I1sol = \frac{200\,cos\,(t)}{8161} + \frac{405\,sin(t)}{8161} + \frac{1612\;{}^{-\frac{81t}{40}}\left(cosh\;\frac{\sqrt{1761}\,t}{40}\right)-\frac{742529\,\sqrt{1761}\,si\;\left(\frac{\sqrt{1761}\,t}{(40)}\right)}{14195421}\Bigg)}{8161}$$

$$Qso1 = \frac{924\;sin(t)}{8161} - \frac{1055\,cos(t)}{8161} + \frac{17377e^{-\frac{81t}{40}}\left(cosh\left(\frac{\sqrt{1761}\,t}{40}\right)+\frac{1109425\,\sqrt{1761}\,sinh\left(\frac{\sqrt{1761}\,t}{(40)}\right)}{30600897}\right)}{8161}$$

3.2. Laplace transform results

Splitting the steady state and transient terms for $Qsol$ and $I1sol$ results in:

$$I1steadystate = \left(\frac{200\,cos\,(t)}{8161}\frac{405\,sin\,(t)}{8161}\right)$$

$$I1steadystate = \frac{1612\;{}^{-\frac{81t}{40}}\left(cosh\left(\frac{\sqrt{1761}\,t}{40}\right)-\frac{742529\,\sqrt{1761}\,sinh\left(\frac{\sqrt{1761}\,t}{(40)}\right)}{14195421}\right)}{8161}$$

The drawing shown in Figure 4 represents the transient (on the left) and steady-state (on the right) behaviors for the current $I1sol$ (a) and the charge $Qsol$ (b) over two unlike periods given by $2 \le t \le 25$ and $0 \le t \le 15$ is shown in, while Figure 5 shows the transient in (a) and steady state in (b) terms.

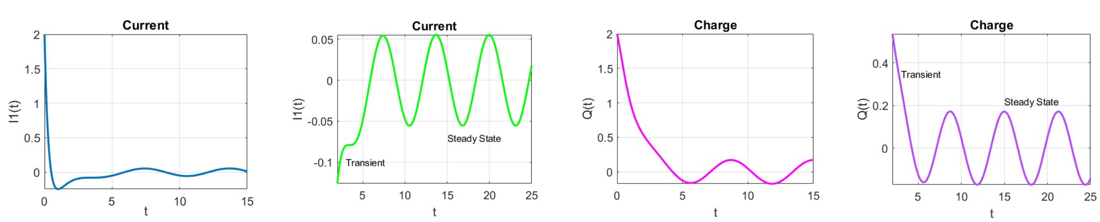

(a) (b)

Figure 4. The transient and steady state behavior for the charge: (a) $Qsol$ and (b) the current $I1sol$ over two unlike time periods given by 2 ≤ t ≤ 25 and 0 ≤ t ≤ 15 respectively

Likewise, splitting $Qsol$ into steady state and transient terms expresses how symbolic computations assist to problem analysis, as given by:

$$Qsteadystate = \left(-\frac{1055\,cos\,(t)}{8161}\frac{924\,sin\,(t)}{8161}\right)$$

$$Qtransient = \frac{1737\quad{}^{-\frac{81t}{40}}\left(cos\ \left(\frac{\sqrt{1761}\,t}{40}\right)+\frac{1109425\sqrt{1761}\,sinh\left(\frac{\sqrt{1761}\,t}{40}\right)}{30600897}\right)}{8161}$$

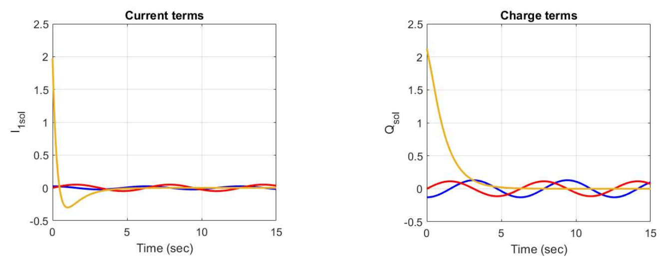

(a) (b)

Figure 5. The transient and steady state terms of; (a) $I1sol$ and (b) $Qsol$

3.3. Comparison results

Figure 6 shows the comparison results between the Laplace transform (LT) and the developed DLCNN of the transient in Figure 6(a), where in Figure 6(b) is steady state. For behaviors for the current *I1sol* and charge *Qsol* over two unlike time periods given by $2 \leq t \leq 25$ (Figure 6(c)) and $0 \leq t \leq 15$ (Figure 6(d)). The modeling DEs of the current $I1sol$ and the capacitor charging $Qso1$ are derived according to the symbolic variables with the circuit element values of Table 1. The charge and current initially decline exponentially. On the other hand, they oscillate over a long period of time. The terms "steady state" and "transient" are used to obtain these characteristics. The qualities of the result can be examined with a symbolic result, but this is not possible with a numeric result. Figure 4 demonstrated that examining $Qsol$ and $I1sol$ visually shows that these equations consist of many terms. The plotting of the behaviors over [0 15] is performed to determine their contributions. The plots in Figure 5 show that $Qsol$ has two steady-state terms and a transient, while I1sol has a steady-state term and transient. From visual inspection, it is noted that $Qsol$ and $I1sol$ are with an exp function term, which is assumed to cause the decay in transient exponentially.

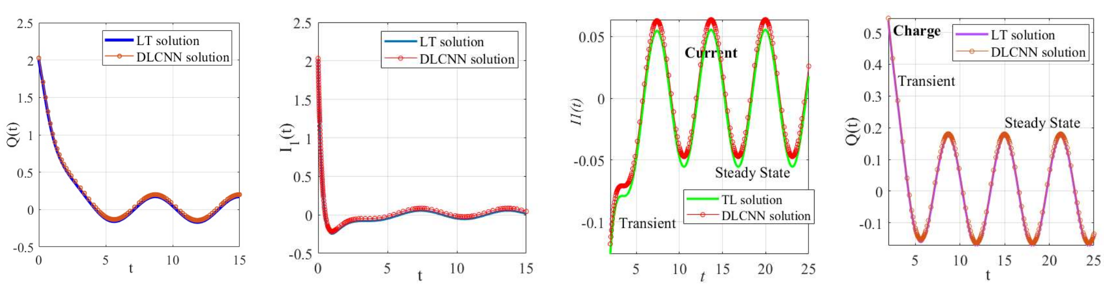

(a) (b) (c) (d)

Figure 6. The comparison of transient and steady-state behavior for (a) the charge $Qsol$ and (b) the current $I1sol$ over two unlike time periods given by; (c) $2 \leq t \leq 25$ and (d) $0 \leq t \leq 15$

The Laplace transform and deep learning CNN solutions show excellent consistency for the steady solutions and there is a good agreement between the obtained transients. Future work can be recommended when comparing the solving of such symbolic differential equations of the 2-loop RLC AC circuit with deep learning convolutional neural network [33], [34].

4. CONCLUSION

This work solves the DEs of a two loops RLC circuit of an alternating voltage source by using Laplace transform. The capacitor charge and current initially decline exponentially and they oscillate over a long period. The qualities of the transient and steady-state results can be examined with a symbolic result, which is not possible with a numeric result. Three major points can be concluded: i) the approach presented has successfully modeled and solved the symbolic differential equations of the currents and the capacitor charging of the 2-loop RLC AC circuit; ii) the visualization of the obtained results of the capacitor charging and inductor current shows that these equations consist of many terms that are assumed to cause the decay in transient exponentially; and iii) this work presented the DLCNN-based solution and compared the results with its corresponding Laplace transform solution.

ACKNOWLEDGMENTS

All authors are acknowledging the University of Information Technology and Communications, Baghdad, Iraq for their assistance and support.

REFERENCES

[1] M. A. Elfouly and M. A. Sohaly, "Van der Pol model in two-delay differential equation representation," *Scientific Reports*, vol. 12, no. 1, p. 2925, Feb. 2022, doi: 10.1038/s41598-022-06911-3.

[2] J. -Aguilar, V. M. -Delgado, M. T. -Hernández, D. Baleanu, R. E. -Jiménez, and M. Al Qurashi, "Analytical Solutions of the Electrical RLC Circuit via Liouville–Caputo Operators with Local and Non-Local Kernels," *Entropy*, vol. 18, no. 8, p. 402, Aug. 2016, doi: 10.3390/e18080402.

[3] F. Battelli and M. Fečkan, "On the existence of solutions connecting singularities in nonlinear RLC circuits," *Nonlinear Analysis: Theory, Methods & Applications*, vol. 116, pp. 26–36, Apr. 2015, doi: 10.1016/j.na.2014.12.015.

[4] I. Y. Korotyeyev and M. Klytta, "The Process Analysis in Domain of Two Variables," *Microsystems, Electronics and Acoustics*, vol. 23, no. 2, pp. 19–24, Apr. 2018, doi: 10.20535/2523-4455.2018.23.2.133701.

[5] M. Bohner, O. Tunç, and C. Tunç, "Qualitative analysis of caputo fractional integro-differential equations with constant delays," *Computational and Applied Mathematics*, vol. 40, no. 6, p. 214, Sep. 2021, doi: 10.1007/s40314-021-01595-3.

[6] A. Atangana and B. S. T. Alkahtani, "Extension of the resistance, inductance, capacitance electrical circuit to fractional derivative without singular kernel," *Advances in Mechanical Engineering*, vol. 7, no. 6, p. 168781401559193, Jun. 2015, doi: 10.1177/1687814015591937.

[7] M. El-Borhamy and A. Ahmed, "Stability Analysis Of Delayed Fractional Integro-Differential Equations With Applications Of RLC Circuits," *Journal of the Indonesian Mathematical Society*, pp. 74–100, Mar. 2020, doi: 10.22342/jims.26.1.795.74-100.

[8] A. Moradi, "Distribution of electromagnetic energy density in a dispersive and dissipative metamaterial," *Journal of Modern Optics*, vol. 68, no. 12, pp. 634–640, Jul. 2021, doi: 10.1080/09500340.2021.1937736.

[9] F. Gómez, J. Rosales, and M. Guía, "RLC electrical circuit of non-integer order," *Open Physics*, vol. 11, no. 10, Jan. 2013, doi: 10.2478/s11534-013-0265-6.

[10] K. A. Abro, A. A. Memon, and A. A. Memon, "Functionality of circuit via modern fractional differentiations," *Analog Integrated Circuits and Signal Processing*, vol. 99, no. 1, pp. 11–21, Apr. 2019, doi: 10.1007/s10470-018-1371-6.

[11] M. Fečkan, "A Survey on the Melnikov Theory for Implicit Ordinary Differential Equations with Applications to RLC Circuits," in *Studies in Systems, Decision and Control*, 2019, pp. 121–160. doi: 10.1007/978-3-030-12232-4_4.

[12] M. El-Borhamy, E. E. M. Rashad, and I. Sobhy, "Floquet analysis of linear dynamic RLC circuits," *Open Physics*, vol. 18, no. 1, pp. 264–277, Jul. 2020, doi: 10.1515/phys-2020-0136.

[13] M. E. Koksal, "Time and frequency responses of non-integer order RLC circuits," *AIMS Mathematics*, vol. 4, no. 1, pp. 64–78, 2019, doi: 10.3934/Math.2019.1.64.

[14] J. Graham and J. Barnes, "A laboratory experience for students of differential equations using RLC circuits," *Primus*, vol. 7, no. 4, pp. 334–340, Jan. 1997, doi: 10.1080/10511979708965875.

[15] N. Geneva and N. Zabaras, "Modeling the dynamics of PDE systems with physics-constrained deep auto-regressive networks," *Journal of Computational Physics*, vol. 403, p. 109056, Feb. 2020, doi: 10.1016/j.jcp.2019.109056.

[16] H. Gao, L. Sun, and J.-X. Wang, "PhyGeoNet: Physics-informed geometry-adaptive convolutional neural networks for solving parameterized steady-state PDEs on irregular domain," *Journal of Computational Physics*, vol. 428, p. 110079, Mar. 2021, doi: 10.1016/j.jcp.2020.110079.

[17] R. Pahič, B. Ridge, A. Gams, J. Morimoto, and A. Ude, "Training of deep neural networks for the generation of dynamic movement primitives," *Neural Networks*, vol. 127, pp. 121–131, Jul. 2020, doi: 10.1016/j.neunet.2020.04.010.

[18] N. Salamat, M. M. S. Missen, and V. B. S. Prasath, "Recent developments in computational color image denoising with PDEs to deep learning: a review," *Artificial Intelligence Review*, vol. 54, no. 8, pp. 6245–6276, Dec. 2021, doi: 10.1007/s10462-021-09977-z.

[19] S. Wei, X. Jin, and H. Li, "General solutions for nonlinear differential equations: a rule-based self-learning approach using deep reinforcement learning," *Computational Mechanics*, vol. 64, no. 5, pp. 1361–1374, Nov. 2019, doi: 10.1007/s00466-019-01715-1.

[20] A. Farahmand, S. Nabi, and D. N. Nikovski, "Deep reinforcement learning for partial differential equation control," in *2017 American Control Conference (ACC)*, IEEE, May 2017, pp. 3120–3127. doi: 10.23919/ACC.2017.7963427.

[21] M. Bocquet, J. Brajard, A. Carrassi, and L. Bertino, "Data assimilation as a learning tool to infer ordinary differential equation representations of dynamical models," *Nonlinear Processes in Geophysics*, vol. 26, no. 3, pp. 143–162, Jul. 2019, doi: 10.5194/npg-26-143-2019.

[22] M. Bocquet, J. Brajard, A. Carrassi, and L. Bertino, "Data assimilation as a deep learning tool to infer ODE representations of dynamical models," *Nonlinear Processes in Geophysics Discussions*, 2019, [Online]. Available: https://npg.copernicus.org/preprints/npg-2019-7/npg-2019-7.pdf

[23] M. Raissi, P. Perdikaris, and G. E. Karniadakis, "Physics-informed neural networks: A deep learning framework for solving forward and inverse problems involving nonlinear partial differential equations," *Journal of Computational Physics*, vol. 378, pp. 686–707, Feb. 2019, doi: 10.1016/j.jcp.2018.10.045.

[24] Y. Khoo, J. Lu, and L. Ying, "Solving parametric PDE problems with artificial neural networks," *European Journal of Applied Mathematics*, vol. 32, no. 3, pp. 421–435, Jun. 2021, doi: 10.1017/S0956792520000182.

[25] K. Mills, M. Spanner, and I. Tamblyn, "Deep learning and the Schrödinger equation," *Physical Review A*, vol. 96, no. 4, p. 042113, Oct. 2017, doi: 10.1103/PhysRevA.96.042113.

[26] W. E, J. Han, and A. Jentzen, "Deep Learning-Based Numerical Methods for High-Dimensional Parabolic Partial Differential Equations and Backward Stochastic Differential Equations," *Communications in Mathematics and Statistics*, vol. 5, no. 4, pp. 349–380, Dec. 2017, doi: 10.1007/s40304-017-0117-6.

[27] I. E. Lagaris, A. Likas, and D. I. Fotiadis, "Artificial neural networks for solving ordinary and partial differential equations," *IEEE Transactions on Neural Networks*, vol. 9, no. 5, pp. 987–1000, 1998, doi: 10.1109/72.712178.

[28] M. L. Piscopo, M. Spannowsky, and P. Waite, "Solving differential equations with neural networks: Applications to the calculation of cosmological phase transitions," *Physical Review D*, vol. 100, no. 1, p. 016002, Jul. 2019, doi: 10.1103/PhysRevD.100.016002.

[29] S. Bajalan and N. Bajalan, "Novel ANN Method for Solving Ordinary and Time-Fractional Black–Scholes Equation," *Complexity*, vol. 2021, pp. 1–15, Jul. 2021, doi: 10.1155/2021/5511396.

[30] R. Bostanabad *et al.*, "Computational microstructure characterization and reconstruction: Review of the state-of-the-art techniques," *Progress in Materials Science*, vol. 95, pp. 1–41, Jun. 2018, doi: 10.1016/j.pmatsci.2018.01.005.

[31] X. Li, Z. Yang, L. C. Brinson, A. Choudhary, A. Agrawal, and W. Chen, "A deep adversarial learning methodology for designing microstructural material systems," in *Proceedings of the ASME Design Engineering Technical Conference*, 2018. doi: 10.1115/DETC201885633.

[32] S. Li, S. Laima, and H. Li, "Data-driven modeling of vortex-induced vibration of a long-span suspension bridge using decision tree learning and support vector regression," *Journal of Wind Engineering and Industrial Aerodynamics*, vol. 172, pp. 196–211, Jan. 2018, doi: 10.1016/j.jweia.2017.10.022.

[33] W. M. Jwaid, Z. S. M. Al-Husseini, and A. H. Sabry, "Development of brain tumor segmentation of magnetic resonance imaging (MRI) using U-Net deep learning," *Eastern-European Journal of Enterprise Technologies*, vol. 4, no. 9(112), pp. 23–31, Aug. 2021, doi: 10.15587/1729-4061.2021.238957.

[34] S. Al-Shoukry, B. J. M. Jawad, Z. Musa, and A. H. Sabry, "Development of predictive modeling and deep learning classification of taxi trip tolls," *Eastern-European Journal of Enterprise Technologies*, vol. 3, no. 3 (117), pp. 6–12, Jun. 2022, doi: 10.15587/1729-4061.2022.259242.

BIOGRAPHIES OF AUTHORS

Inaam Rikan Hassan was born in Baghdad, Iraq. She received the B.Sc. degree in mathematical science from Baghdad University, Baghdad, Iraq, in 1992, and the M.Sc. degree in mathematical science/numerical analysis also from Baghdad University, Baghdad, Iraq in 2004, She received her Ph.D. degree in mathematical science/application of differential equations from Saint Petersburg State University Russia in 2008. Her research interests include numerical analysts, applications of differential equations in movement, statistics. She has published researches in international journals including Scopus. She has contributed as member of several organization committees in many conferences. She can be contacted at: drinrh@uitc.edu.iq.

Ghuson S. Abed was born in Baghdad, Iraq. She received his B.Sc. and M.Sc. degrees in mathematics from the University of Al-Mustansiriya-Baghdad, Iraq, in 1991 and 2015, respectively. She has taught many subjects in her field of specialization. She is the author of more than 4 articles published in international journals, and her research interests focus on the field of solving partial differential equations using numerical solution and transforms integral. She can be contacted at: Ghsonabed.2019@uitc.edu.iq.

Ahmad H. Sabry was born in Baghdad, Iraq. He received his B.Sc. and M.Sc. degrees in electrical and electronics, control and automation, and engineering from the University of Technology-Baghdad, Iraq, in 1994 and 2001, respectively. He received a Ph.D. degree in DC-based PV-powered home energy systems from the Department of Electrical and Electronic Engineering, control, and Automation at UPM, Malaysia in 2017. He is the author of more than 35 articles, and more than 5 inventions, and holds one patent. His research interests include integrated solar powered smart home system based on voltage matching, DC distribution, industrial robotic systems, and wireless energy management systems. He is a reviewer in more than three ISI journals. He can be contacted at email: ahs4771384@gmail.com.